P H Y S I C A L   R E V I E W   L E T T E R S

Quantum Simulation of Energy Transport with Embedded Rydberg Aggregates

D. W. Schönleber,[1] A. Eisfeld,[1] M. Genkin,[1] S. Whitlock,[2] and S. Wüster[1]

[1]*Max Planck Institute for the Physics of Complex Systems, Nöthnitzer Strasse 38, 01187 Dresden, Germany*
[2]*Physikalisches Institut, Universität Heidelberg, Im Neuenheimer Feld 226, 69120 Heidelberg, Germany*

We show that an array of ultracold Rydberg atoms embedded in a laser driven background gas can serve as an aggregate for simulating exciton dynamics and energy transport with a controlled environment. Energetic disorder and decoherence introduced by the interaction with the background gas atoms can be controlled by the laser parameters. This allows for an almost ideal realization of a Haken-Reineker-Strobl-type model for energy transport. The transport can be monitored using the same mechanism that provides control over the environment. The degree of decoherence is traced back to information gained on the excitation location through the monitoring, turning the setup into an experimentally accessible model system for studying the effects of quantum measurements on the dynamics of a many-body quantum system.

Introduction.—Excitation transport through dipole-dipole interactions [1,2] plays a prominent role in diverse physical settings, including photosynthesis [3,4], exciton transport through quantum-dot arrays [5], and molecular aggregates [6–8]. Of crucial importance is the competition between the fundamentally coherent transport mechanism and the coupling to the environment, which has been under intense scrutiny in the context of photosynthesis (e.g., [1,9–13]) and recently experienced a resurgence of interest (e.g., [14–19]). Often, clean studies of excitation transport are impeded by the large number of degrees of freedom in these systems, for example, strongly coupled vibrational modes [9,20]. Ultracold atoms prepared in highly excited Rydberg states exhibit similar dipolar state-changing interactions [21–26] as found in organic molecules, but are considerably simpler to study. Because of their strong interactions and relative ease to control using lasers, Rydberg atoms have been proposed as quantum simulators for quantum spin models [27,28] and electron-phonon interactions [29]. Aggregates formed by networks of Rydberg atoms (Rydberg aggregates) [30,31] are also ideally suited to the study of dipolar energy transport in an experimentally accessible system, as recently demonstrated [32].

Here we study energy transport through a Rydberg aggregate embedded within an optically driven background gas that acts as a precisely controlled environment. This system extends the one recently used to observe diffusive excitation transport [32] by separating the aggregate degrees of freedom from those of the background gas. The background gas is electromagnetically rendered transparent for a probe beam. Only in the vicinity of the aggregate atoms, interactions disrupt this transparency, causing each aggregate atom to cast a shadow with radius given by the interaction strength. We demonstrate parameters for which a larger absorption shadow is cast by the

atom carrying an excitation, allowing us to infer its location. We show that the background gas simultaneously causes a backaction on the aggregate that can give rise to non-Gaussian disorder as well as site-dependent dephasing. The resulting excitation transfer dynamics can be described by a master equation similar to the one introduced by Haken-Reineker-Strobl (HRS) [33–35] to study the transition from coherent to incoherent transport.

The experimental realization of a controllable HRS-type model will benefit the study of excitation transport in an open system, be it semiconductors or light harvesting. For the latter, extensions to exciton-vibrational coupling and non-Markovian environments may be required [9,20,30,36,37]. Finally, we show how decoherence in this system is intimately linked to the information obtained by the background gas acting as a quantum measurement device. In particular, despite strong aggregate-background interactions, decoherence vanishes if the background atoms do not allow one to infer the location of the excitation.

Scheme and model.—The system we propose consists of a chain of N Rydberg atoms with spacing d forming the aggregate sketched in Fig. 1. Such an arrangement can be created by exciting Rydberg states from a trapped ultracold atomic gas using tightly focused laser beams [38,39], or by pulsed or chirped excitation in the dipole blockade regime [40,41], which gives rise to spatially correlated Rydberg excitation patterns [42–51]. $N - 1$ atoms are initially prepared in the state $|s\rangle = |\nu s\rangle$ with principal quantum number ν and angular momentum $l = 0$, while a single atom is excited to the state $|p\rangle = |\nu p\rangle$, with angular momentum $l = 1$. This $|p\rangle$ excitation can then migrate through the aggregate through resonant dipole-dipole exchange interactions [22,23]. In addition, the aggregate is immersed in a gas of M background atoms, initially prepared in the electronic ground state $|g\rangle$, the positions of which could be random or arranged in a regular fashion.
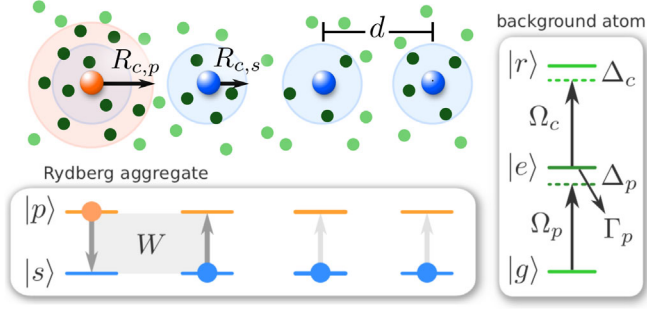
FIG. 1 (color online).　Sketch of an embedded Rydberg aggregate. An assembly of several Rydberg atoms in a state $|s\rangle$ (large blue) and one in a state $|p\rangle$ (large orange) is linearly arranged with spacing d in a background atomic gas (shades of green). These background atoms are then addressed with an EIT scheme (right panel), providing detection signals within radii $R_{c,s/p}$ around each aggregate atom.

These atoms are coupled by two laser fields from $|g\rangle$ via a short-lived intermediate state $|e\rangle$ (spontaneous decay rate Γ_p) to a third Rydberg level, $|r\rangle = |\nu's\rangle$ [52–58]. Aggregate and background atoms could be the same or different atomic species.

This system is governed by the many-body Lindblad master equation for the density matrix $\hat{\rho}$ ($h = 1$)

$$\dot{\hat{\rho}} = -i[\hat{H}, \hat{\rho}] + \sum_\alpha \mathcal{L}_{\hat{L}_\alpha}[\hat{\rho}]. \qquad (1)$$

The Hamiltonian consists of three parts, $\hat{H} = \hat{H}_{\mathrm{agg}} + \hat{H}_{\mathrm{EIT}} + \hat{H}_{\mathrm{int}}$, for the aggregate, the background gas of three-level atoms and van der Waals (vdW) interactions [23,59,60] between atoms that are in a Rydberg state. The superoperator $\mathcal{L}_{\hat{L}_\alpha}[\hat{\rho}]$ describes spontaneous decay of the background atom α from level $|e\rangle$, thus $\mathcal{L}_{\hat{O}}[\hat{\rho}] = \hat{O}\hat{\rho}\hat{O}^\dagger - (\hat{O}^\dagger\hat{O}\hat{\rho} + \hat{\rho}\hat{O}^\dagger\hat{O})/2$ and the decay operator is $\hat{L}_\alpha = \sqrt{\Gamma_p}\hat{\sigma}_{ge}^{(\alpha)}$, with $\hat{\sigma}_{kk'}^{(\alpha)} = [|k\rangle\langle k'|]_\alpha$ acting on atom α only and $k, k' \in \{g, e, r, s, p\}$.

The aggregate atoms are labeled by Latin indices such as n and m. Restricted to the Hilbert space with a single excitation and setting the constant energy splitting between s and p to zero, we can write

$$\hat{H}_{\mathrm{agg}} = \sum_{n \neq m} W_{nm}\hat{\sigma}_{sp}^{(n)}\hat{\sigma}_{ps}^{(m)} = \sum_{n \neq m} W_{nm}|\pi_n\rangle\langle\pi_m|, \qquad (2)$$

where $|\pi_n\rangle = |ss...p...ss\rangle$ (all aggregate atoms are in $|s\rangle$ except the nth, which is in $|p\rangle$) and $W_{nm} = C_3/|r_n - r_m|^3$. Here, C_3 is the dipole-dipole interaction strength and r_n is the position of aggregate atom n. We call eigenstates of (2) excitons [61,62]. For simplicity, we have ignored vdW interactions between aggregate atoms [63].

The Hamiltonian for the background gas in the rotating wave approximation reads

$$\hat{H}_{\mathrm{EIT}} = \sum_\alpha \left[\frac{\Omega_p}{2}\hat{\sigma}_{eg}^{(\alpha)} + \frac{\Omega_c}{2}\hat{\sigma}_{re}^{(\alpha)} + \mathrm{H.c.} \right.$$
$$\left. - \Delta_p\hat{\sigma}_{ee}^{(\alpha)} - (\Delta_p + \Delta_c)\hat{\sigma}_{rr}^{(\alpha)} \right], \qquad (3)$$

where $\Omega_{p,c}$ and $\Delta_{p,c}$ are the probe and coupling Rabi frequencies and detunings, respectively. Typically $\Omega_p \ll \Omega_c$ and $\Delta_p + \Delta_c = 0$, which corresponds to conditions of electromagnetically induced transparency (EIT) used for Rydberg atom detection [32,64].

Background atoms interact among themselves and with the aggregate through vdW interactions

$$\hat{H}_{\mathrm{int}} = \sum_{\alpha < \beta} V_{\alpha\beta}^{(rr)}\hat{\sigma}_{rr}^{(\alpha)}\hat{\sigma}_{rr}^{(\beta)} + \sum_{a \in \{s,p\}, \alpha n} V_{\alpha n}^{(ra)}\hat{\sigma}_{rr}^{(\alpha)}\hat{\sigma}_{aa}^{(n)}. \qquad (4)$$

For simplicity we assume isotropic interactions. To use the background gas as a probe for the state of the aggregate it is necessary that the interactions are state dependent. The interaction strength between two atoms α, n is $V_{\alpha n}^{(ra)} = V^{(ra)}(|r_\alpha - r_n|) = C_{\eta(a),ra}/|r_\alpha - r_n|^{\eta(a)}$, when they are in states $|r\rangle$ and $|a\rangle \in \{|s\rangle, |p\rangle\}$. As concrete examples we consider $|s\rangle = |43s\rangle$, $|p\rangle = |43p\rangle$ in ^{87}Rb, with two choices $|r\rangle = |38s\rangle$ or $|r'\rangle = |17s\rangle$ for the upper state of the EIT ladder. The former realizes power laws $\eta(a) = 6, 6, 4$ for $a = r, s, p$, respectively, with $|V^{(rp)}| \gg |V^{(rs)}|$, due to a nearly resonant process: $43p + 38s \leftrightarrow 41d + 38p$ [65], and the latter has $\eta(p) = 6$ and $V^{(rp)} \approx V^{(rs)}$.

Excitation detection.—On resonance ($\Delta_{p,c} = 0$), the background gas becomes transparent for the probe beam described by Ω_p. However, close to the aggregate atoms, interactions $V_{\alpha n}^{(ra)} > V_c = \Omega_c^2/(2\Gamma_p)$ destroy the transparency [32,64] (see also [66]). This creates an absorption shadow around each aggregate atom, the radius $R_{c,a} = (2C_{\eta(a),ra}\Gamma_p/\Omega_c^2)^{1/\eta(a)}$ of which depends on the state $a \in \{s, p\}$, as sketched by blue (orange) circles in Fig. 1. Through this difference we can infer the location of the p excitation.

Effective aggregate model.—To derive an effective model for the aggregate alone we proceed by adiabatically eliminating the internal states of the background atoms following the approach described in Ref. [67]. This is justified when the time scale on which background atoms would approach a steady state, set by the atomic decay rate $1/\Gamma_p$, is shorter than that for excitation transport $1/W(d) = d^3/C_3$ (for details, see [68]). The evolution of the reduced aggregate density matrix $\hat{\rho}^{(\mathrm{agg})} = \sum_{nm}\rho_{nm}|\pi_n\rangle\langle\pi_m|$, in the case $\Delta_{p,c} = 0$, $V_{\alpha\beta}^{(rr)} = 0$ and to leading order in Ω_p, obeys

$$\dot{\hat{\rho}}^{(\mathrm{agg})} = -i[\hat{H}_{\mathrm{agg}} + \hat{H}_{\mathrm{eff}}, \hat{\rho}^{(\mathrm{agg})}] + \sum_\alpha \mathcal{L}_{\hat{L}_{\mathrm{eff}}^{(\alpha)}}[\hat{\rho}^{(\mathrm{agg})}], \qquad (5)$$

$$\hat{H}_{\text{eff}} = \sum_n \left[\sum_\alpha \frac{\Omega_p^2}{\Omega_c^2} \frac{\bar{V}_{n\alpha}}{1 + (\bar{V}_{n\alpha}/V_c)^2} \right] |\pi_n\rangle\langle\pi_n|, \quad (6)$$

$$\hat{L}_{\text{eff}}^{(\alpha)} = \sum_n \left[\frac{\Omega_p}{\sqrt{\Gamma_p}} \frac{1}{i + V_c/\bar{V}_{n\alpha}} \right] |\pi_n\rangle\langle\pi_n|, \quad (7)$$

where we have introduced the background-aggregate interaction $\bar{V}_{n\alpha} = V_{n\alpha}^{(rp)} + \sum_{m \neq n} V_{m\alpha}^{(rs)}$. Note the imaginary contributions to $\hat{L}_{\text{eff}}^{(\alpha)}$. For the case $\Delta_{p,c} \neq 0$, see [68].

The effective Hamiltonian (6) describes a mean energy shift of aggregate site n due to the interaction with the level $|r\rangle$ of the background atoms, weighted by the steady-state occupation of $|r\rangle$. The strength of the second term (7) is set by the two-level atom photon scattering rate $\gamma_{\text{eff}} \approx \Omega_p^2/\Gamma_p$ within the critical radius of an aggregate atom. Imaginary off-diagonal terms in (5) arising from imaginary parts of (7) can be interpreted as a contribution to the disorder [68], while real ones describe dephasing mechanisms. The relative contributions of disorder and dephasing terms can be controlled by choosing Rydberg states with different interactions and through the EIT laser parameters. Equation (5) furnishes a Haken-Reineker-Strobl-type model [35] for excitation transport. All scenarios from dominant dephasing to dominant disorder can be realized by varying the intermediate state detuning Δ_p while keeping the two-photon detuning fixed: $\Delta_p + \Delta_c \approx 0$. In particular, for large Δ_p the contribution of dephasing can be significantly reduced, see [68].

In the following, we analyze the influence of the disorder and dephasing introduced by the background gas. More explicitly, Eq. (5) reads $\dot{\rho}_{nm} = \sum_k i(W_{km}\rho_{nk} - W_{nk}\rho_{km}) + i(E_m - E_n + \epsilon_{nm})\rho_{nm} - \gamma_{nm}\rho_{nm}/2$, with $E_n = \sum_\alpha H_{\text{eff}}^{(n\alpha)}$, $\epsilon_{nm} = \sum_\alpha \text{Im}[L_{\text{eff}}^{(n\alpha)} L_{\text{eff}}^{(m\alpha)*}]$, and $\gamma_{nm} = \sum_\alpha(|L_{\text{eff}}^{(n\alpha)}|^2 + |L_{\text{eff}}^{(m\alpha)}|^2 - 2\text{Re}[L_{\text{eff}}^{(n\alpha)} L_{\text{eff}}^{(m\alpha)*}])$. We then define distributions $P_E(E_n - \langle E_n\rangle)$, $P_\epsilon(\epsilon_{nm} - \langle\epsilon_{nm}\rangle)$ and $P_\gamma(\gamma_{nm})$, for the probability with which an individual background atom α contributes to disorder and dephasing in an ensemble average over background atom positions [E_n disorder from (6), ϵ_{nm} disorder from (7), P_γ dephasing]. Both the width and the shape of these distributions can be controlled by the laser parameters and the background atom density. In Fig. 2 we show two examples: panel (a) corresponds to resonant EIT excitation ($\Delta_{p,c} = 0$) and large background gas density, resulting in dominant dephasing and Gaussian distributions, while panel (b) shows the case of finite intermediate state detuning and low density such that interactions between probe and aggregate atoms are weaker. Detuning from the intermediate level reduces spontaneous decay and makes dephasing weaker than disorder. Remarkably, for low densities and weak interactions we find significant outliers in the atomic distance distribution that cause non-Gaussian disorder that can
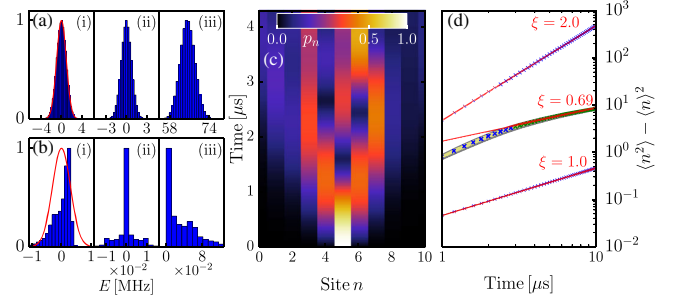
FIG. 2 (color online). Varying disorder and dephasing in quantum simulations of energy transport. (a) Histograms for disorder and dephasing (i) P_E, (ii) P_ϵ, (iii) P_γ, using parameters $\Omega_p = 1.3$ MHz, $\Omega_c = 30$ MHz, $\Delta_p = \Delta_c = 0$, $\Gamma_p = 6.1$ MHz, $d = 19\ \mu$m, $W(d) = 0.24$ MHz, $\rho_{\text{bg}} = 3.8 \times 10^{18}\ \text{m}^{-3}$, $C_{4,rp} = -1032\ \text{MHz}\,\mu\text{m}^4$, $C_{6,rs} = -87\ \text{MHz}\,\mu\text{m}^6$, thus assuming an upper background level $|r\rangle$. (b) The same as (a), with parameters $\Omega_p = 12$ MHz, $\Omega_c = 90$ MHz, $\Delta_p = -20$ MHz, $\Delta_c = 22$ MHz, $d = 24\ \mu$m, $W(d) = 0.1$ MHz, $\rho_{\text{bg}} = 9.5 \times 10^{17}\ \text{m}^{-3}$, $C_{6,rp} = -0.4\,\text{MHz}\,\mu\text{m}^6$, $C_{6,rs} = -0.1\ \text{MHz}\,\mu\text{m}^6$, thus assuming an upper background level $|r\rangle$. (c) Effect of disorder on a single transport realization, using parameters as in (b). (d) Variance of the excitation location ($\times$), fit by $\sigma_n^2(t) = St^\xi$. From bottom to top parameters as in (a), (b) with $N = 31$, (a) with $\Omega_p = 0$.

crucially modify excitation transport [69]. By controlling the placement of individual background atoms using microstructured optical traps, even more exotic forms of disorder could be studied.

The effects of disorder and dephasing on transport can be seen in Fig. 2(c), where we show a single realization of Eq. (5) for $N = 11$ atoms immersed in a gas of randomly but homogeneously distributed background atoms. In a corresponding ensemble average, the spatial width of the excitation distribution over aggregate sites $\sigma_n^2 = \langle n^2\rangle - \langle n\rangle^2$ carries the transport signatures Fig. 2(d). Parametrizing $\sigma_n^2(t) = St^\xi$, we find $\xi = 2$ for ballistic transport ($\Omega_p = 0$), $\xi = 1$ for typical diffusive transport resulting from Fig. 2(a) and $\xi = 0.69$ for subdiffusive transport arising from the non-Gaussian disorder in Fig. 2(b).

Imaging and measurement-induced decoherence.—The degree of decoherence present in this system is intimately linked to the action of the background gas acting as a real-time probe of the aggregate, making it an appealing model to demonstrate measurement-induced decoherence [70]. Since the background gas degrees of freedom have been eliminated in the effective model, we demonstrate this effect with simulations of the full master equation, which also serve to verify model (5). We study an aggregate with $N = 3$, probed by two randomly distributed pairs of background atoms, using a quantum-jump Monte Carlo technique [71,72]. The background atom pairs have a separation $\Delta r = 0.3\ \mu$m, yielding $V^{(rr)}(\Delta r) = 730$ MHz [73]
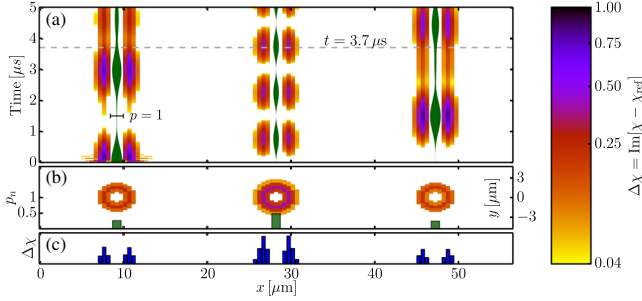
FIG. 3 (color online). Link between absorption signature and excitation transport. (a) Difference in optical response between dynamic and empty aggregate $\Delta\chi(x) = \mathrm{Im}[\chi - \chi_{\mathrm{ref}}]$ during transport, normalized by the two-level ($|g\rangle$, $|e\rangle$) response. Green lines indicate the location of aggregate atoms r_n and their thickness the population p_n. (c) Snapshot of $\Delta\chi(x)$ at $t = 3.7$ μs. (b) Visualization of the corresponding two-dimensional signal [74], green bars indicate p_n. Here, $\Omega_p = 0.2$ MHz, otherwise parameters as in Fig. 4.

FIG. 4 (color online). Exciton transport in a continuously monitored embedded Rydberg aggregate. Geometries are shown in the top panels. (a) Site occupations p_n for $n = 1, 2, 3$ (solid red, dashed blue, dot-dashed black lines) in a nondecohering case, $\Omega_p = 1.3$ MHz, $\Omega_c = 30$ MHz, $d = 19$ μm, $\delta = 0.6$ μm, other parameters as in Fig. 2(a). Color-matched crosses show the populations according to the effective model, Eq. (5). The orange line counts the number of scattered photons $n_{\mathrm{phot}}(t) = \int dt \Gamma_p \sum_\alpha \mathrm{Tr}(\hat{\rho}(t)[|e\rangle\langle e|]_\alpha)$. (b) The same for a strongly decohering case with $\delta = 1.5$ μm, other parameters as in (a).

to include significant interactions between background atoms. We initially prepare the aggregate in state $|\pi_1\rangle$ and all background atoms in their ground state $|g\rangle$.

Each background atom α heralds the arrival of an aggregate excitation through the optical susceptibility $\chi_\alpha(t) = \Gamma_p/\Omega_p \mathrm{Tr}(\hat{\rho}\hat{\sigma}_{eg}^{(\alpha)})$, the imaginary part of which yields the optical absorption. The average optical susceptibility of the background gas $\chi(x)$ is approximated by spatial binning of the $\chi_\alpha(t)$ from many simulations. To monitor the excitation transport, one can infer the locaion of the $|p\rangle$ state by subtracting from $\chi(x)$ a reference signal $\chi_{\mathrm{ref}}(x)$ corresponding to the absorption of an inactive aggregate (chain of only $|s\rangle$ states) as in [32]. We see in Fig. 3 that the resulting signal is directly linked to the probability distribution of the excitation $p_n(t) = \mathrm{Tr}(\hat{\rho}|\pi_n\rangle\langle\pi_n|)$. These simulations also show that background-background interactions $V_{\alpha\beta}^{(rr)}$ are relatively benign for the chosen states and densities.

The dephasing of the aggregate depends strongly on the position of the background atoms. In particular, a given background atom only provides significant information on the excitation location if it is located in a ring *between* the two critical radii $R_{c,s} < r < R_{c,p}$ as visible in Fig. 3. This is demonstrated in Fig. 4 where we place one background atom at a distance δ from each site as shown in the top panels. For $\delta < R_{c,s}$ background atoms permanently scatter a large number of photons, nonetheless the aggregate dynamics proceeds coherently [panel (a)]. In contrast, for $R_{c,s} < \delta < R_{c,p}$, despite a smaller total number of scattered photons, aggregate decoherence is strong.

The connection between information provided by the scattered photon and decoherence is explicit in the quantum-jump algorithm: The inset of Fig. 4(b) shows for a single realization how the state of the aggregate p_2

(blue dashed) is linked to quantum jumps of the $|e\rangle$ population of its probe atom (green). This link only occurs when the state of the background atom and the state of the aggregate are significantly entangled in the moment of spontaneous decay. Since this is not the case in panel (a), single trajectories (not plotted) there show no effect of quantum jumps on the state of the aggregate.

Conclusions and outlook.—We have shown that a Rydberg aggregate embedded in an optically coupled background gas realizes a flexible quantum simulator of a Haken-Reineker-Strobl-type model for energy transport. Site-dependent dephasing and disorder can be controlled through laser intensities, frequencies, and background atomic density. Furthermore, this system could be extended to study other fundamental features believed to be at play in photosynthetic light harvesting: We have seen evidence for non-Markovian features and nontrivial relaxation when the time scale on which the background atoms reach their steady state is made comparable to transport time scales, a regime not discussed here. The analogue of internal molecular vibrations could be engineered as in Ref. [29]. Disorder distributions could be controlled even further using an additional class of background atoms [75]. All these features would extend the HRS-type model proposed here to quantum simulations of light-harvesting processes in a similar spirit but with complementary technology to the proposals of Refs. [37,76,77]. Decoherence of the aggregate arises through continuous monitoring of the location of the excitation, providing a hands-on example of measurement-induced decoherence of a quantum state. Further applications of this system could be monitoring and decoherence of adiabatic excitation transport involving external (motional) degrees of freedom [78,79].

[1] J. Franck and E. Teller, J. Chem. Phys. **6**, 861 (1938).
[2] J. Frenkel, Phys. Rev. **37**, 17 (1931).
[3] R. van Grondelle and V. I. Novoderezhkin, Phys. Chem. Chem. Phys. **8**, 793 (2006).
[4] H. van Amerongen, L. Valkunas, and R. van Grondelle, *Photosynthetic Excitons* (World Scientific, Singapore, 2000).
[5] C. R. Kagan, C. B. Murray, and M. G. Bawendi, Phys. Rev. B **54**, 8633 (1996).
[6] S. K. Saikin, A. Eisfeld, S. Valleau, and A. Aspuru-Guzik, Nanophotonics **2**, 21 (2013).
[7] S. Kirstein and S. Daehne, Int. J. Photoenergy **2006**, 20363 (2006).
[8] T. Förster, in *Quantum Efficiency in Complex Systems, Part II: From Molecular Aggregates to Organic Solar Cells, Semiconductors and Semimetals*, edited by U. Würfel, M. Thorwart, and E. R. Weber (Academic Press, San Diego, 2011), p. 47.
[9] T. Renger, V. May, and O. Kühn, Phys. Rep. **343**, 137 (2001).
[10] T. Förster, Ann. Phys. (Berlin) **437**, 55 (1948).
[11] T. Förster, in *Modern Quantum Chemistry*, edited by Sinanoğlu (Academic Press, New York, 1965), Chap. III B 1, p. 93.
[12] G. Scheibe, Naturwissenschaften **25**, 795 (1937).
[13] H. van Amerongen, L. Valkunas, and R. van Grondelle, *Photosynthetic Excitons* (World Scientific, Singapore, 2000).
[14] G. S. Engel, T. R. Calhoun, E. L. Read, T.-K. Ahn, T. Mančal, Y.-C. Cheng, R. E. Blankenship, and G. R. Fleming, Nature (London) **446**, 782 (2007).
[15] M. B. Plenio and S. F. Huelga, New J. Phys. **10**, 113019 (2008).
[16] M. Mohseni, P. Rebentrost, S. Lloyd, and A. Aspuru-Guzik, J. Chem. Phys. **129**, 174106 (2008).
[17] M. Milder, B. Brüggemann, R. van Grondelle, and J. Herek, Photosynth. Res. **104**, 257 (2010).
[18] T. Scholak, T. Wellens, and A. Buchleitner, Eur. Phys. Lett. **96**, 10001 (2011).
[19] T. Scholak, F. de Melo, T. Wellens, F. Mintert, and A. Buchleitner, Phys. Rev. E **83**, 021912 (2011).
[20] G. Ritschel, J. Roden, W. T. Strunz, and A. Eisfeld, New J. Phys. **13**, 113034 (2011).
[21] W. R. Anderson, J. R. Veale, and T. F. Gallagher, Phys. Rev. Lett. **80**, 249 (1998).
[22] F. Robicheaux, J. V. Hernandez, T. Topcu, and L. D. Noordam, Phys. Rev. A **70**, 042703 (2004).
[23] T. F. Gallagher, *Rydberg Atoms* (Cambridge University Press, Cambridge, England, 1994).

[24] H. Park, E. S. Shuman, and T. F. Gallagher, Phys. Rev. A **84**, 052708 (2011).
[25] D. Barredo, H. Labuhn, S. Ravets, T. Lahaye, A. Browaeys, and C. S. Adams, arXiv:1408.1055.
[26] S. Ravets, H. Labuhn, D. Barredo, L. Béguin, T. Lahaye, and A. Browaeys, Nat. Phys. **10**, 914 (2014).
[27] H. Weimer, M. Müller, I. Lesanovsky, P. Zoller, and H. P. Büchler, Nat. Phys. **6**, 382 (2010).
[28] I. Lesanovsky, Phys. Rev. Lett. **108**, 105301 (2012).
[29] J. P. Hague and C. MacCormick, New J. Phys. **14**, 033019 (2012).
[30] A. Eisfeld and J. S. Briggs, Chem. Phys. **281**, 61 (2002).
[31] O. Mülken, A. Blumen, T. Amthor, C. Giese, M. Reetz-Lamour, and M. Weidemüller, Phys. Rev. Lett. **99**, 090601 (2007).
[32] G. Günter, H. Schempp, M. Robert-de-Saint-Vincent, V. Gavryusev, S. Helmrich, C. S. Hofmann, S. Whitlock, and M. Weidemüller, Science **342**, 954 (2013).
[33] H. Haken and P. Reineker, Z. Phys. **249**, 253 (1972).
[34] H. Haken and G. Strobl, Z. Phys. **262**, 135 (1973).
[35] A. Eisfeld and J. S. Briggs, Phys. Rev. E **85**, 046118 (2012).
[36] F. C. Spano, Acc. Chem. Res. **43**, 429 (2010).
[37] S. Mostame, P. Rebentrost, A. Eisfeld, A. J. Kerman, D. I. Tsomokos, and A. Aspuru-Guzik, New J. Phys. **14**, 105013 (2012).
[38] F. Nogrette, H. Labuhn, S. Ravets, D. Barredo, L. Béguin, A. Vernier, T. Lahaye, and A. Browaeys, Phys. Rev. X **4**, 021034 (2014).
[39] M. Schlosser, S. Tichelmann, J. Kruse, and G. Birkl, Quantum Inf. Process. **10**, 907 (2011).
[40] D. Jaksch, J. I. Cirac, P. Zoller, S. L. Rolston, R. Côté, and M. D. Lukin, Phys. Rev. Lett. **85**, 2208 (2000).
[41] M. D. Lukin, M. Fleischhauer, R. Côté, L. M. Duan, D. Jaksch, J. I. Cirac, and P. Zoller, Phys. Rev. Lett. **87**, 037901 (2001).
[42] T. Pohl, E. Demler, and M. D. Lukin, Phys. Rev. Lett. **104**, 043002 (2010).
[43] M. Gärttner, K. P. Heeg, T. Gasenzer, and J. Evers, Phys. Rev. A **88**, 043410 (2013).
[44] H. Weimer, R. Löw, T. Pfau, and H. P. Büchler, Phys. Rev. Lett. **101**, 250601 (2008).
[45] S. Wüster, J. Stanojevic, C. Ates, T. Pohl, P. Deuar, J. F. Corney, and J. M. Rost, Phys. Rev. A **81**, 023406 (2010).
[46] I. Lesanovsky and J. P. Garrahan, Phys. Rev. A **90**, 011603 (2014).
[47] S. Bettelli, D. Maxwell, T. Fernholz, C. S. Adams, I. Lesanovsky, and C. Ates, Phys. Rev. A **88**, 043436 (2013).
[48] R. M. W. van Bijnen, S. Smit, K. A. H. van Leeuwen, E. J. D. Vredenbregt, and S. J. J. M. F. Kokkelmans, J. Phys. B **44**, 184008 (2011).
[49] H. Schempp, G. Günter, M. Robert-de-Saint-Vincent, C. S. Hofmann, D. Breyel, A. Komnik, D. W. Schönleber, M. Gärttner, J. Evers, S. Whitlock *et al.*, Phys. Rev. Lett. **112**, 013002 (2014).
[50] P. Schauß, M. Cheneau, M. Endres, T. Fukuhara, S. Hild, A. Omran, T. Pohl, C. Gross, S. Kuhr, and I. Bloch, Nature (London) **491**, 87 (2012).
[51] P. Schauß, J. Zeiher, T. Fukuhara, S. Hild, M. Cheneau, T. Macrí, T. Pohl, I. Bloch, and C. Gross, arXiv:1404.0980.

[52] I. Friedler, D. Petrosyan, M. Fleischhauer, and G. Kurizki, Phys. Rev. A **72**, 043803 (2005).

[53] A. K. Mohapatra, T. R. Jackson, and C. S. Adams, Phys. Rev. Lett. **98**, 113003 (2007).

[54] S. Mauger, J. Millen, and M. P. A. Jones, J. Phys. B **40**, F319 (2007).

[55] A. K. Mohapatra, M. G. Bason, B. Butscher, K. J. Weatherill, and C. S. Adams, Nat. Phys. **4**, 890 (2008).

[56] H. Schempp, G. Günter, C. S. Hofmann, C. Giese, S. D. Saliba, B. D. DePaola, T. Amthor, M. Weidemüller, S. Sevinçli, and T. Pohl, Phys. Rev. Lett. **104**, 173602 (2010).

[57] S. Sevinçli, C. Ates, T. Pohl, H. Schempp, C. S. Hofmann, G. Günter, T. Amthor, M. Weidemüller, J. D. Pritchard, D. Maxwell *et al.*, J. Phys. B **44**, 184018 (2011).

[58] V. Parigi, E. Bimbard, J. Stanojevic, A. J. Hilliard, F. Nogrette, R. Tualle-Brouri, A. Ourjoumtsev, and P. Grangier, Phys. Rev. Lett. **109**, 233602 (2012).

[59] K. Singer, J. Stanojevic, M. Weidemüller, and R. Côté, J. Phys. B **38**, S295 (2005).

[60] L. Béguin, A. Vernier, R. Chicireanu, T. Lahaye, and A. Browaeys, Phys. Rev. Lett. **110**, 263201 (2013).

[61] V. May and O. Kühn, *Charge and Energy Transfer Dynamics in Molecular Systems* (Wiley-VCH, Berlin, 2001).

[62] C. Ates, A. Eisfeld, and J. M. Rost, New J. Phys. **10**, 045030 (2008).

[63] H. Zoubi, A. Eisfeld, and S. Wüster, Phys. Rev. A **89**, 053426 (2014).

[64] G. Günter, M. Robert-de-Saint-Vincent, H. Schempp, C. S. Hofmann, S. Whitlock, and M. Weidemüller, Phys. Rev. Lett. **108**, 013002 (2012).

[65] For these quantum numbers we obtain dispersion coefficients $C_{6,rr} = 3.67 \times 10^{18}$ au, $C_{6,rs} = -6 \times 10^{17}$ $C_{4,rp} = -2 \times 10^{10}$ from exact diagonalization of the diatomic Hamiltonian, in agreement with [59]. Because of the resonance, V_{rp} has several significant dispersion coefficients, the R^{-4} form has been chosen to reproduce the same critical radius $R_{c,p}$ as the full interaction for our parameters.

[66] B. Olmos, W. Li, S. Hofferberth, and I. Lesanovsky, Phys. Rev. A **84**, 041607(R) (2011).

[67] F. Reiter and A. S. Sorensen, Phys. Rev. A **85**, 032111 (2012).

[68] See Supplemental Material at http://link.aps.org/supplemental/10.1103/PhysRevLett.114.123005 for the derivation of Eqs. (5)–(7), details of EIT and disorder parametrization.

[69] S. M. Vlaming, V. A. Malyshev, A. Eisfeld, and J. Knoester, J. Chem. Phys. **138**, 214316 (2013).

[70] A. N. Korotkov and D. V. Averin, Phys. Rev. B **64**, 165310 (2001).

[71] K. Mølmer, Y. Castin, and J. Dalibard, J. Opt. Soc. Am. B **10**, 524 (1993).

[72] D. W. Schönleber, M. Gärttner, and J. Evers, Phys. Rev. A **89**, 033421 (2014).

[73] For practical reasons we cut off state energies at $V_{max} = 600$ MHz. This still amounts to a full Rydberg blockade.

[74] The simulation only featured a one-dimensional distribution of background atoms. To visualize the expected experimental signal, we compute from the one-dimensional absorption signal around each aggregate atom $\chi_{1D}(\delta) = \chi_{1D}(x - x_n)$ the corresponding two-dimensional signal $\chi(x, y) = \chi(\mathbf{r}) \equiv \chi_{1D}(\delta)$, with $\delta = |\mathbf{r} - \mathbf{r}_n|$, where $\mathbf{r} = (x, y)^T$.

[75] S. Möbius and A. Eisfeld (to be published).

[76] F. Herrera and R. V. Krems, Phys. Rev. A **84**, 051401(R) (2011).

[77] F. Herrera, K. W. Madison, R. V. Krems, and M. Berciu, Phys. Rev. Lett. **110**, 223002 (2013).

[78] S. Wüster, C. Ates, A. Eisfeld, and J. M. Rost, Phys. Rev. Lett. **105**, 053004 (2010).

[79] S. Möbius, S. Wüster, C. Ates, A. Eisfeld, and J. M. Rost, J. Phys. B **44**, 184011 (2011).